A Theory of Withdrawal of Cylinders from Liquid Baths

DAVID A. WHITE and JOHN A. TALLMADGE

Yale University, New Haven, Connecticut

A theory of the amount of liquid entrained by cylinders upon withdrawal from liquid baths is derived for a wide range of cylinder radii. The theory is based on matching curvatures for static and dynamic menisci. Predicted values are expressed as the effect of the dimensionless wire radius (Goucher number) and dimensionless withdrawal speed (capillary number) on the dimensionless flux.

The theory was verified experimentally for all wire radii by removing short cylinders from oily fluids and with other information. The fluids used included kerosene, mineral oil, motor oil, and glycerine, with viscosities from 2 to 500 centipoise; Goucher numbers ranged from 0.05 to 1.2. Deviations, which were noted at high capillary numbers where velocity gradients become appreciable, indicated that the theory is a plug flow or low speed theory. Also discussed are differences found with water and the conditions under which films coalesced into droplets.

The first known general description of cylinder withdrawal has only recently been published (*6*). Conditions and restrictions on the problem are given in that paper, but in the interest of clarity are summarized here.

The problem of concern is the vertical constant-speed withdrawal of cylinders from quiescent baths of laminar Navier-Stokes fluids. It is also limited to cases where the liquid-gas interface in the meniscus is free of waves, ripples, or other instabilities. These conditions are not very restrictive; many of the important coating, pickling, and lubrication applications are described by this motion. Figure 1 is a sketch of the withdrawal process from a free surface *GH*. When a wire of radius R is withdrawn at a velocity u_w from a wetting liquid having constant fluid properties, the entrained film has a constant external radius s_o at a point A some distance above the liquid meniscus.

The problem is the determination of the quantity of the liquid entrained per unit time Q, which is given by the relation

$$Q = 2\pi \int_R^{s_o} urdr \qquad (1)$$

where u is the vertical velocity of the fluid element having a radial position r. Here the flux Q is a function of the film radius s_o and thereby a function of withdrawal speed, cylinder radii, gravity, and fluid properties. These independent variables are best characterized for design purposes (*6*) by two groups: the dimensionless withdrawal speed N_{Ca} and the dimensionless wire radius N_{Go}.

By defining a dimensionless flux $\overline{T}$, the problem can be restated as one of predicting the functional relationship denoted by Equation (2).

$$\overline{T} = \overline{T}\,(N_{Ca}, N_{Go}) \qquad (2)$$

Here $\overline{T}$ is related to Q by defining a flux radius $\overline{s}$ and from it the dimensionless flux. Thus

$$Q \equiv \pi u_w\,(\overline{s}^2 - R^2) \qquad (3)$$

$$\overline{T} \equiv (\overline{s} - R)\left(\frac{\rho g}{\mu u_w}\right)^{1/2} \qquad (4)$$

David White is with Cambridge University, Cambridge, England. John A. Tallmadge is with Drexel Institute, Philadelphia, Pennsylvania.

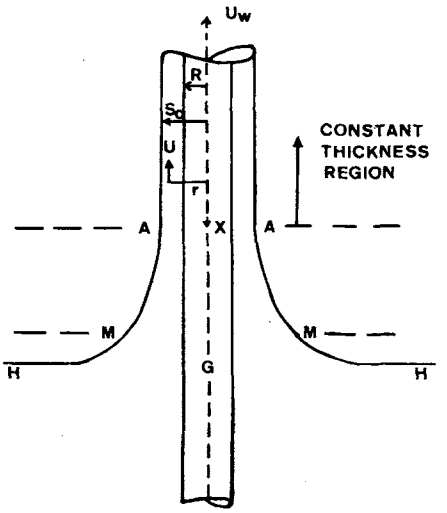

Fig. 1. Withdrawal of a cylinder from a liquid bath.

This flux radius $\overline{s}$ is that which would result from solidifying the film; it is also the thickness of a hypothetical film in which the velocity profile is uniform and the flux is identical to the actual film. In practice $\overline{s}$ is often almost as large as s_o.

LITERATURE

The three flow regimes for cylinder withdrawal (*6*) are: (1) the special case of *small wires* or low Goucher, that is, where $N_{Go} \leq 0.04$; (2) the more general region of *large wires* or intermediate Goucher; and (3) the special case of large cylinders or *flat plates*, called high Goucher; here $N_{Go} \geq 2$.

No methods have been described for predicting cylinder withdrawal theoretically for all Goucher numbers. The only successful theoretical approach is that described for the special case of flat plates; that is, the approach of Landau–Levich (*3, 4*). Their work applies where $N_{Go} \to \infty$; in flux form (*1*) with a more accurate constant (*10*), their result is

$$\overline{T} = 0.944\,N_{Ca}^{1/6}\,(1 - 0.297\,N_{Ca}^{1/3}) \qquad (5)$$

Data reported for large cylinders and flat plates agree with Equation (5) at low speeds ($10^{-4} < N_{Ca} < 0.03$). However, at higher speeds ($0.03 < N_{Ca} < 10$), the fluxes predicted from Equation (5) are larger than experimental values (*7, 10*) by more than 5%.

Some small wire data have been reported by Goucher and Ward (*2*). Their empirical correlation for wires of $0.003 < N_{Go} < 0.04$ may be expressed as

$$(\bar{s}/R) - 1 = 4.8\, N_{Ca} \qquad (6a)$$

The equivalent expression in $\bar{T}$ notation is

$$\bar{T} = 6.8\, N_{Ca}^{1/2}\, N_{Go} \qquad (6b)$$

Unfortunately, however, this correlation was developed and tested for a narrow range of speed ($0.04 < N_{Ca} < 0.35$).

Data for the intermediate range of large wires are very sparse and imprecise. Some results have recently appeared for a few speeds, $0.1 < N_{Ca} < 1.0$ at two Goucher numbers (0.11 and 0.25). With these empirical values a rough prediction of the shape of Equation (2) has been presented in graphical form (*6*). However, too many regions of Goucher and capillary numbers remain untested to allow much confidence in such an empirical correlation.

PURPOSE

The object of this paper is to extend the empirical work of Tallmadge, Labine, and Wood (*6*) by presenting a theoretical prediction for the flux of liquid entrained during cylinder withdrawal for a wide range of Goucher numbers. The theory used is an extension of the matching approach developed by Landau–Levich for flat plates (*3, 4*). The region of validity of this theory is also presented, based on experimental evidence.

THEORETICAL SOLUTION

The matching approach involves equating two approximate expressions for curvature of the liquid-gas interface at some point on the meniscus, such as at M in Figure 1. These expressions are based on equations of motions near M. The equation of motion *above* M is based on viscous and surface tension terms in the AM region and viscous and gravity terms above A, leading to a dynamic meniscus curvature $(d^2s/dx^2)_D$. The equation of motion *below* M is based on surface tension and gravity terms, leading to a static meniscus curvature $(d^2s/dx^2)_S$. The locations are indicated in the match equation which, for a cylinder, is

$$\lim_{s\to\infty}\left(\frac{d^2s}{dx^2}\right)_D = \lim_{s\to s_o}\left(\frac{d^2s}{dx^2}\right)_S \qquad (7)$$

The curvature at the top of the status meniscus on the outside of a cylinder is a function of σ, ρ, g, and radius of the surface support. For Goucher numbers less than 3, this curvature has been shown (*9*) to be

$$\lim_{s\to R}\left(\frac{d^2s}{dx^2}\right)_S = \frac{2}{a}\left[\frac{2.4\, N_{Go}^{0.85}}{1 + 2.4\, N_{Go}^{0.85}} + \frac{0.5}{N_{Go}}\right] \qquad (8)$$

Equation (8) was developed by fitting theoretical values which had been calculated numerically. Equation (8) is accurate to 1% at $N_{Go} = 3$, becomes much more precise as $N_{Go} \to 0$, and agrees with theory in the $N_{Go} \to \infty$ limit. This function has been experimentally verified (*9*) by comparison of theoretical meniscus profiles with measured profiles on large wires ($0.2 < N_{Go} < 1.6$).

The proper surface support radius for withdrawal is s_o, the external radius of the film in the constant thickness region. Thus the static curvature appropriate for matching is that at $s \to s_o$. Therefore, replacing R/a with s_o/a, the proper curvature for use in Equation (7) is given by

$$\lim_{s\to s_o}\left(\frac{d^2s}{dx^2}\right)_S = \frac{2}{a}\left[\frac{2.4\, N_{Go}^{0.85}(s_o/R)^{0.85}}{1 + 2.4\, N_{Go}^{0.85}(s_o/R)^{0.85}} + \frac{0.5}{N_{Go}(s_o/R)}\right] \qquad (9)$$

The limiting curvature of the dynamic meniscus was determined by modifying the flat plate result. The latter is based on solving a one-dimensional, simplified, third-order, Navier-Stokes equation for the AM region (Figure 1), using the boundary conditions at A for three initial conditions. The approximate solution for a flat plate, for which the film thickness is h, is given (*3, 4, 8*) as

$$\lim_{h\to\infty}\left(\frac{d^2h}{dx^2}\right)_D \doteq \frac{0.642\,(3N_{Ca})^{2/3}}{h_o} \qquad (10)$$

Equation (10) may be applied to a cylinder by replacing h_o with $s_o - R$. Thus

$$\lim_{s\to\infty}\left(\frac{d^2s}{dx^2}\right)_D \doteq \frac{0.944\sqrt{2}\,N_{Ca}^{2/3}}{(s_o - R)} \qquad (11)$$

Equation (11) implies a negligible contribution of the curvature in the nearly horizontal plane, as well as the assumptions implicit in Equation (10).

Matching Equations (9) and (11) in Equation (7) and invoking the definition of T_o, one obtains

$$T_o = \frac{0.944\, N_{Ca}^{1/6}}{\left[\dfrac{2.4\, N_{Go}^{0.85}\,(s_o/R)^{0.85}}{1 + 2.4\, N_{Go}^{0.85}\,(s_o/R)^{0.85}} + \dfrac{0.5}{N_{Go}\,(s_o/R)}\right]} \qquad (12a)$$

Equation (12*a*) is the desired theoretical solution. It is, however, not in convenient form, since T_o and s_o are both expressions for film thickness. It may be placed in explicit form for T_o by noting that (s_o/R), by definition of T_o, is the following function:

$$s_o/R = 1 + \frac{T_o}{N_{Go}}\left(\frac{N_{Ca}}{2}\right)^{1/2} \qquad (12b)$$

Elimination of (s_o/R) from Equations (12*a*) and (12*b*) leads to the explicit form

$$T_o = L_o\,(N_{Ca}, N_{Go}) \qquad (13)$$

Numerical values for Equation (13) are given in Table 1. These were obtained by solving Equations (12*a*) and

TABLE 1. PREDICTED FILM THICKNESSES IN $T_o \times 10^3$*

Tabular values of theoretical Equation (13)

$$T_o = L_o\,(N_{Ca}, N_{Go})$$

N_{Go}	N_{Ca}, 0.0001	N_{Ca}, 0.0003	N_{Ca}, 0.001	N_{Ca}, 0.003	N_{Ca}, 0.01	N_{Ca}, 0.03	N_{Ca}, 0.1	N_{Ca}, 0.3	N_{Ca}, 0.1
∞†	203	244	299	359	438	526	643	772	944
3.0	198	238	291	350	427	514	629	757	930
1.0	169	203	248	298	366	442	549	677	864
0.6	141	170	208	250	309	377	477	607	815
0.3	96	115	141	171	213	265	351	486	738
0.1	39	47	58	70	88	113	162	275	625
0.06	24	29	36	43	55	70	103	192	584
0.03	12	15	18	22	28	36	53	107	542
0.01	4	5	6	7	9	12	18	38	506

* For region of validity, see experimental results and Figure 7.
† Identical to values from Equation (5) for flat plates.

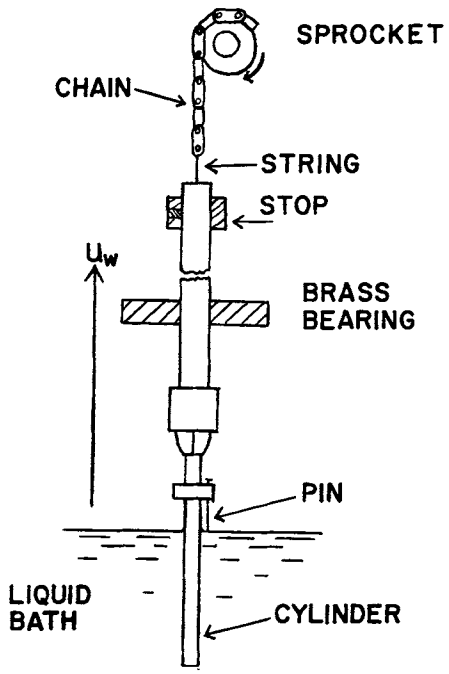

Fig. 2. The apparatus for withdrawal of short cylinders.

(12*b*) on a digital computer by an iteration process; a slide rule would not be accurate enough. Initially, T_o was set at 0.2 and successive approximations for T_o were calculated for a fixed N_{Ca} and N_{Go} using Equations (12*b*), then (12*a*), and then repeating. The solution usually converged to within 0.0001 in T_o in two to five iterations. Ten or more iterations were often required in the region where $\partial T/\partial N_{Ca}$ is large, such as where $0.1 < N_{Ca} < 1.0$ and $N_{Go} < 0.1$ simultaneously.

The theoretical solution [Equation (13)] was expressed in the desired flux form by invoking the relationship between flux and thickness for cylinders (*6*); in *s* form, this relationship is

$$\left(\frac{\bar{s}}{R}\right)^2 = \left(\frac{s_o}{R}\right)^2 - \frac{N_{Go}^2}{N_{Ca}} \left[\left(\frac{s_o}{R}\right)^4 \left\{\ln\frac{s_o}{R} - \frac{3}{4}\right\} + \left(\frac{s_o}{R}\right)^2 - \frac{1}{4}\right] \quad (14)$$

The value of $\bar{T}$ was then calculated by Equation (15), the $\bar{T} - \bar{s}$ relationship which follows from Equation (4), and definitions of capillary and Goucher numbers.

$$\bar{T} \equiv \left(\frac{\bar{s}}{R} - 1\right)\left(\frac{2}{N_{Ca}}\right)^{1/2} N_{Go} \quad (15)$$

In this way the desired explicit function for flux, described by Equation (16), was calculated numerically from Equations (12) to (15).

$$\bar{T} = \bar{L}\,(N_{Ca}, N_{Go}) \quad (16)$$

EXPERIMENTAL METHOD

Since the data available in the region most important for testing the theory ($0.04 < N_{Go} < 2$) are sparse and imprecise, $\bar{T}$ values were determined experimentally. The detailed method (*8*) is summarized below.

The mass of fluid adhering to wires was measured gravimetrically after removal from immersion depths of 5 to 35 cm.; a gravimetric technique (*2*) was used because it is more accurate than a photographic one (*6*). The wires were held in a ¼-in. chuck attached to ½ drill rod which was constrained to move vertically by a brass bearing (see Figure 2). Driven by a variable speed motor through a length of string, chain, and a sprocket wheel, the rod and wires were withdrawn at 0.2 to 11 cm./sec. at the following speeds: 0.183, 0.599, 0.995, 1.59, 3.76, 4.56, 5.55, 7.56, 9.53, or 11.5 cm./sec. The room temperature was held constant at 23.4° ± 0.2°C. by an air conditioner.

Table 2. Fluid Properties at 23.4°C.

Fluid symbol	Description of the fluid	Viscosity μ, poise	Density ρ, g./cc.	Surf. ten.* σ, dynes/cm.	Cap length a, cm.
G	Glycerine	5.13	1.259	64.8	0.324
S	Shell motor oil (Vitrea 69)	4.86	0.901	29.8	0.260
L	Mineral oil (heavy, USA)	1.56	0.880	31.4	0.270
KL	Kerosene-mineral oil mixture (40% kerosene)	0.151	0.840	27.8	0.260
GW	Glycerine-water (50% glycerine)	0.131	1.164	67.9	0.345
K	Kerosene	0.0167	0.792	26.4	0.261
W	Water	0.00932	0.998	71.7	0.383
Estimated precision		±1%	±0.1%	±0.5%	±0.2%

* Calculated from a using g = 980 cm./sec.^{2}. Thus $\sigma = 490\ \rho a^2$.

The properties of the seven fluids used to test the theory are given in Table 2. Except for the capillary viscometer measurements, which were made in an ± 0.1°C. bath, these properties were measured in the same constant-temperature room in which withdrawal was measured. Other properties were measured in a capillary rise apparatus (capillary length) and with a hydrometer (density). A 20 × 20 cm. metal tank 35 cm. deep was used as the liquid bath container for flux measurements.

With these ranges of fluid properties and withdrawal speeds values of capillary numbers from 0.0002 to 1 were obtained.

The wire specimens were chosen to give Goucher numbers from 0.05 to 1.2; precise values for each group of runs are shown in Table 3. For the small wires, labeled 5 and 4, it was found necessary to use a cluster of four shorter wires to retain rigidity without sacrificing precision in the flux measurement. The ends of the specimens were filed flat and perpendicular to the wire axis.

For a test run, the wire was first immersed to a given depth. This was adjusted carefully until a pinpoint just touched the free surface of the liquid, resulting in a depth precision of about ± 0.25 cm. Immediately after the wire was removed from the bath, a watch glass was placed underneath to catch any drops. The wire and watch glass were then weighed and the mass of liquid removed was calculated. The process was

Table 3. Cylinder Radii and Goucher Numbers

Wire No.	3	1	2	5	4
Material	Glass	Brass	Brass	Copper	Copper
Radius, cm.	0.346	0.318	0.0795	0.0248	0.0140
No. of wires	1	1	1	4	4
Immersion depths, cm.	5, 10, 15	5, 10, 15*	5, 10, 15*	34.5	31.2
N_{Go} numbers (approx.)	1.2	1.2	0.3	0.1	0.05
N_{Go} numbers (precise)					
Fluid *G*	—	—	—	—	0.043
Fluid *S*	—	1.22	0.306	0.0954	0.054
Fluid *L*	—	1.18	0.294	0.0919	0.052
Fluid *KL*	—	1.23	—	—	—
Fluid *GW*	1.00	—	—	—	—
Fluid *K*	—	1.22	0.305	—	—
Fluid *W*	0.902	—	—	—	—

* The immersion depths used for wires 1 and 2 in fluid *L* (mineral oil) were 5, 10, and 20 cm.; for wire 2 in fluid *S* (Shell motor oil) a single immersion depth of 15 cm. was used.

repeated and in most cases the mass of flux was reproduced to within 2%.

End effects were calculated from measurements taken at three immersion lengths. Since end effects at steady state are independent of immersion length, the total mass entrained was plotted vs. immersion length. Straight lines resulted, which verified steady state. The slopes of these plots were used to calculate fluxes, since the slopes are equivalent to entrainment per unit length. The maximum error in slope was estimated to be 4%. End effects, indicated by the intercepts, were usually small or negligible.

Table 3 indicates the immersion lengths used for each run; end effects for very small wires, 5 and 4, were so small that variation of immersion lengths was not used.

Another way of eliminating end effects is the use of Morey's method (7). It involves plotting the ratio of mass withdrawn to immersion length against the reciprocal of immersion length and extrapolating to infinite length of immersion; the intercept on this plot is equal to the withdrawal per unit length, that is, flux. Morey's method was not used, however, because the extrapolation was found to be curved in some cases; these curvatures occurred where end effects were comparatively large, such as for low capillary numbers.

In view of the matching theory used, the shape of the dynamic meniscus is of interest. As wires were pulled out of the liquid, it was generally observed that the liquid meniscus was not distorted greatly, if at all; such distortion that did occur was greatest at large N_{Go} and N_{Ca}.

One other aspect of cylinder withdrawal of practical importance is the formation of droplets on the wires, which occurs primarily with small wires. Because drops formed several centimeters above the bath curved meniscus, however, they did not influence the analysis in this paper. Nevertheless, further tests were made to determine the conditions under which drops form.

Although films were stable for all runs made at $N_{Go} = 0.3$ and higher, the films disintegrated into droplets for all runs at the low N_{Go} values of 0.05. At $N_{Go} = 0.1$, drops were formed in high-speed runs (resulting in large thicknesses) but not at lower speeds. The influence of film thickness on film stability was then studied for N_{Go} of 0.08 to 0.16; critical values of N_{Ca} were found for each N_{Go} tested.

EXPERIMENTAL RESULTS

Experimental fluxes for Goucher numbers of approximately 0.5, 0.1, 0.3, and 1.2 are given numerically in Tables 4 to 7* and graphically in Figures 3 to 6, respectively. In addition to flux results in the $\overline{h}/R$ and $\overline{T}$ forms, theoretically predicted values of $\overline{T}$ and $\overline{h}/h_o$, as well as experimental conditions of N_{Go} and N_{Ca}, are also included in Tables 4 to 7 for each run. The actual speeds used (u_w) can be determined from tabular values of N_{Ca} and the fluid property data from Table 2. Estimated values of film thickness (h_o) can be determined from tabular values of $\overline{h}/R$ and $\overline{h}/h_o$ together with wire radii from Table 3.

Runs 103, 104, and 105 of Table 6 ($N_{Go} \doteq 0.3$, fluid S motor oil) were taken forty days after runs 56, 57, and 58; they indicated that the flux reproducibility was good: $\pm$ 3, $\pm$ 2, and $\pm$ 1% in these three cases.

Comparison of theoretical and experimental values of flux, as shown in Figures 3 to 6, indicates that the theory describes withdrawal entrainment for the entire range of radii studied and for a wide range of low and intermediate speeds. (The fluid G data of Figure 3 actually agree within 12% of theory for speeds below N_{Ca} of 0.3, as shown in Table 4. The apparent discrepancy for these glycerine data in Figure 3 is due to differences in Goucher number.) This confirmation of theory is noted over a

* Tabular material has been deposited as document 8702 with the American Documentation Institute, Photoduplication Service, Library of Congress, Washington 25, D. C., and may be obtained for $1.25 for photoprints or 35-mm. microfilm.

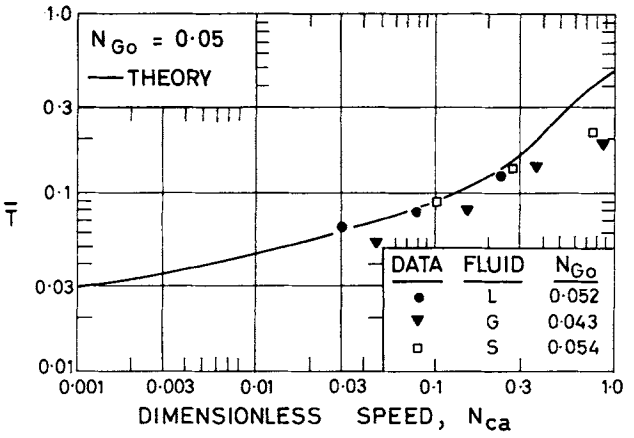

Fig. 3. Experimental results for the smallest wires (0.014 cm. radius).

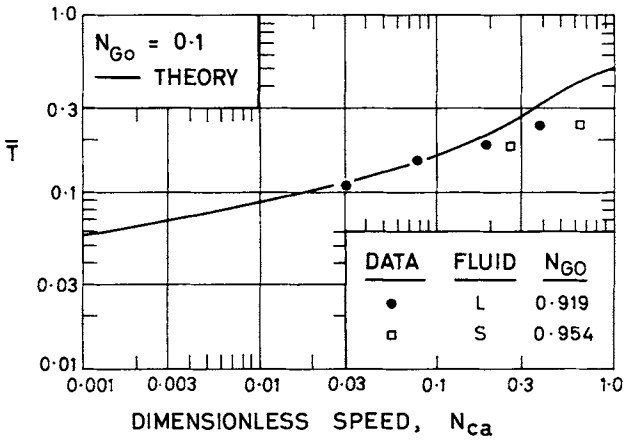

Fig. 4. Experimental results (0.0248 cm. radius wires).

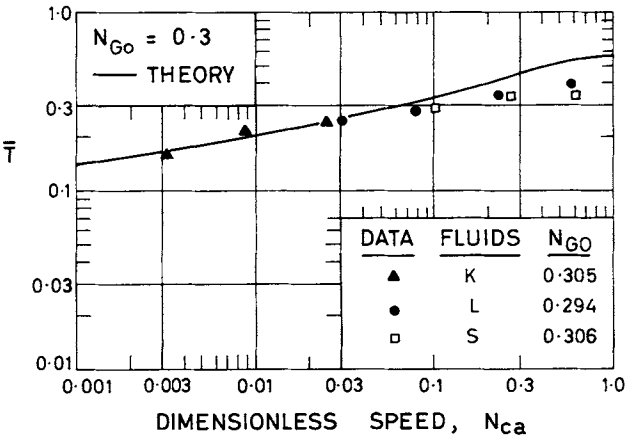

Fig. 5. Experimental results (0.0795 cm. radius wires).

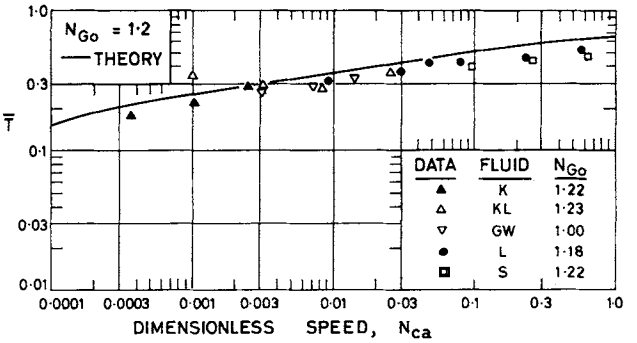

Fig. 6. Experimental results for rods (0.318 and 0.346 cm. radii).

twenty-fivefold range of N_{Go} in the intermediate N_{Go} range, which is the most difficult to predict (*6*). Based on this evidence and that from flat plates (*10*), it is believed that this theory is applicable for all wire radii, that is, all N_{Go}.

The deviation between theory and experiment which occurs at high speeds, such as shown in Figure 5, indicates that the theory denoted by Equations (12*a*), (13), and (16) may be called a *low-speed* theory. Care should be used to avoid applying this name too strictly, however, as the theory is applicable over wide ranges of capillary number. As shown in Figures 3 to 6, the theory is accurate over at least a one hundredfold range of N_{Ca} and is probably valid for speeds lower than were measured as well.

Although the theory developed here is valid for all N_{Go} and a very wide range of N_{Ca}, determination of the quantitative limits of validity is an important practical problem. It was partly for this reason that many of the experiments were run at "high" speeds.

The data in Figures 4 and 5 clearly indicate that the deviation, which exists between theory and experiment at high speeds, tends to become larger at higher speeds. (The same trend is noted with the small wire data of Figure 3 when the glycerine data are compared at the same Goucher numbers.) Because of this gradual increase in deviation with speed, it is not possible to determine a region of validity without specifying a criterion of precision desired. For a precision criterion of 14%, chosen to be larger than experimental scatter, the data in Tables 4 to 6 (and noted in Figures 3 to 5) indicate that the theory is valid up to capillary numbers of about 0.3, 0.2 and 0.09 at Goucher numbers of 0.05, 0.1, and 0.3, respectively. It is interesting to note that the maximum deviation of all fifteen runs taken within these speed limits is within the precision criterion; the median deviation is 5%.

The data reported in Figure 6 (rods) scatter somewhat more than those in Figures 3 to 5 and do not tend to deviate as much at higher speeds. Thus a definite limit on validity is difficult to establish at $N_{Go} = 1.2$, based on these data. This does not present a difficulty, however, because the limit at $N_{Go} \to \infty$ (flat plates) has been established by previous work (*10*), as described previously in the Literature Section. This limit on flat plates, that is, at $N_{Ca} = 0.03$, is taken as more reliable than any that might be estimated from the data of Figure 6.

Consideration of the limits on validity for $N_{Go} \to \infty$ and $N_{Go} = 0.3$ indicates that the limit for $N_{Go} = 1.2$ lies between a capillary number of 0.03 and 0.09. The data of Figure 6 substantiate this conclusion.

In summary, the theory applies up to a capillary number of 0.03 for all wire sizes; for smaller wires ($N_{Go} \leq 0.1$), it applies over a broader range, that is, up to about $N_{Ca} = 0.2$. For the twenty-six runs taken in these regions,

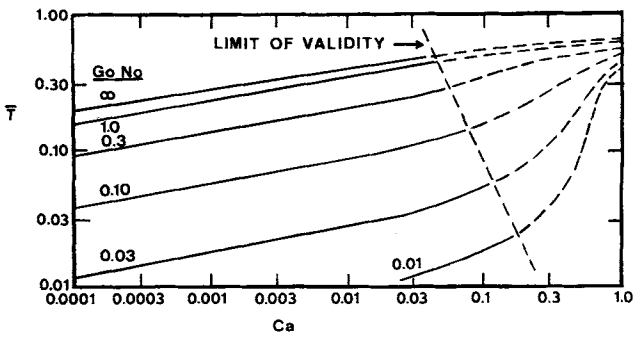

Fig. 7. Prediction of entrained liquid on cylinders, low-speed theory [Equation (16)].

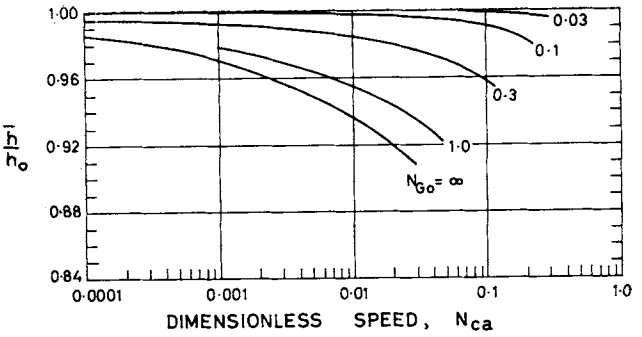

Fig. 8. Deviation from plug flow (theoretical).

the median deviation of $\bar{T}$ between theory and experiment was 9%. The approximate region of validity of the theory is shown graphically in Figure 7 in the flux or $\bar{T}$ form of Equation (16).

Several runs were made with distilled water to check the report (*5*) that in one test, the water flux predicted by flat plate theory was only about half that found by experiment. In seven runs at $0.0002 < N_{Ca} < 0.0015$ and $N_{Go} = 0.9$, the paradoxical behavior of water was confirmed. The values predicted from theory were 30 to 50% below experimental values. Additional tests with high purity, deionized water, 250 p.p.m. detergent, and a trace amount of dye in the water failed to indicate any differences in the deviation between theory and experiment. On the other hand, runs with a 50-50 aqueous mixture of glycerine and water behaved similarly to the oil tests and the theory of this work. Several reasons for this water paradox have been proposed: surface roughness, dynamic surface tension, and thin layers, but none of these hypotheses is satisfactory. Thus the deviations for withdrawal from water are currently unexplained.

DISCUSSION OF PLUG FLOW

The ratio of $\bar{h}$ to h_o is a convenient expression for determining whether plug flow is approached in any film in question; it is a normalized quantity. When $\bar{h}/h_o$ has a value of nearly one, the film may be described as having a uniform velocity which is also almost equal to the wire velocity, as in plug flow.

Values of $\bar{h}/h_o$, calculated from this theory, are plotted as functions of capillary number at lines of constant Goucher number in Figure 8. In the wide ranges where this theory has been found to be applicable, it is seen that nearly all films are closely approximated by a plug flow model. (Since these theoretical predictions of $\bar{h}/h_o$ are, of course, not reliable in the high-speed ranges where the theory is inaccurate, none of these high-speed values have been included in Figure 8).

Figure 8 also shows an appreciable influence of radii (N_{Go}) on the deviation from plug flow at a given speed (N_{Ca}). This influence of Goucher number seems related to the effect of Goucher number on the upper limit of N_{Ca} for which the theory has been found to be valid.

With values of $\bar{h}/h_o$ for each experimental run, as given in Tables 4 to 7, accurate estimates of film thicknesses may be made for the region in which the film thickness is constant with height. Such estimates indicate that this low-speed theory is valid over at least a fortyfold range of film thickness, that is, from 0.006 mm. (kerosene, run 80K) to 0.24 mm. (mineral oil, run 1L).

The early flat plate theory of Landau and Levich (*3, 4*) was a solid flow theory based on a negligible effect of gravity in both the dynamic meniscus and constant

thickness regions (AM and above A, respectively, in Figure 1). This analysis was extended by Derjaguin and Titiyevskava (*1*), who corrected for gravity-induced velocity gradients in the constant thickness region but not in the meniscus; it may be called a plug flow model. The cylinder theory presented here as Equations (13) and (16) is a plug flow theory of the Derjaguin-Titiyevskava type; In order to extend this analysis to higher speeds and to correct for gravity in the meniscus, further work is planned along the lines used successfully for flat plates (*10*)

The expression for the plug flow theory for cylinders, like the similar Russian work for flat plates, exhibits the peculiar property of having a maximum value of $\overline{T}$ on a $\overline{T}$ vs. N_{Ca} plot (one maximum for each N_{Ca}). Since these maxima occur only at high speeds of $N_{Ca} = 1$, however, and are above the region of N_{Ca} for which the theory is valid, the existence of these maxima is not important practically. On the other hand, they do show the need for avoiding extrapolations.

SPECIAL CASES

The theory is compared below with the literature of flat plates and small wires. No comparison is possible with the few points reported at intermediate Goucher numbers (*6*), since the speeds used in that work were above those applicable for this theory.

Flat plates: For large cylinders and flat plates, where $N_{Go} \to \infty$, Equation (12*a*) reduces to $T_o = 0.944\ N_{Ca}^{1/6}$ which, in terms of $\overline{T}$, is identical to Equation (5) of flat plate theory.

Small wires: Where $N_{Go} \to 0$, Equation (12*a*) reduces to

$$T_o = 2\ (0.944)\ N_{Ca}^{1/6}\ N_{Go}\ (s_o/R) \qquad (17)$$

Substituting Equation (17) into (12*b*) and rearranging, one obtains the explicit form

$$\frac{h_o}{R} = \frac{s_o}{R} - 1 = \frac{1.33\ N_{Ca}^{2/3}}{1 - 1.33\ N_{Ca}^{2/3}} \qquad (18)$$

In T notation, the equivalent of Equation (18) is

$$T_o = N_{Go}\left(\frac{1.89\ N_{Ca}^{1/6}}{1 - 1.33\ N_{Ca}^{2/3}}\right) \qquad (19)$$

Since plug flow is approached as $N_{Go} \to 0$, $\overline{T} \to T_o$ for small wires. Thus, the flux equation for small wires is

$$\overline{T} = N_{Go}\left(\frac{1.89\ N_{Ca}^{1/6}}{1 - 1.33\ N_{Ca}^{2/3}}\right) \qquad (20)$$

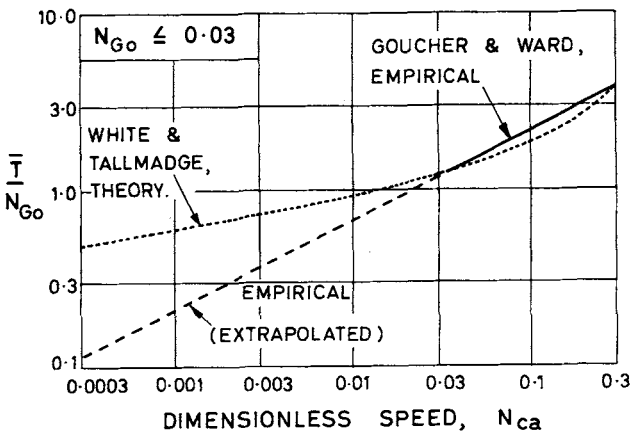

Fig. 9. Comparison of small wire theory with smoothed data. *a.* Small wire theory given by Equation (20). *b.* Empirical correlation given by Equation (6*b*), measured at $0.04 \leq N_{Ca} \leq 0.30$.

Equation (20) indicates that $\overline{T}$ is linear in N_{Go} at low N_{Go}; this condition appears in Figure 7. Comparison of the low-speed theories for the general case and for small wires [Equation (16) vs. Equation (20), respectively] indicates that this small wire theory is accurate, within about 5%, up to $N_{Go} = 0.06$ if N_{Ca} is 0.1 or less. The extent of validity of Equation (20) varies slightly with N_{Go}; the $\overline{T}$ value is accurate to within 5% up to higher speeds such as $N_{Ca} = 0.5$ if N_{Go} is less than 0.01 and up to $N_{Go} = 0.10$ if at low speeds such as $N_{Ca} \sim 0.0001$.

Values from this small wire theory [Equation (20)] are compared with the Goucher and Ward's empirical correlation [Equation (6*b*)] in Figure 9. The good agreement of the theory with previous data is additional confirmation of the low-speed theory [Equation (16)] as well as this special case of a small wire theory [Equation (20)]. The functional dependence of flux on N_{Ca} indicated by Goucher and Ward's data is, in this region, similar to that found theoretically. The flux data are generally somewhat higher than the theory (4%, 16%, and 13% at capillary numbers of 0.04, 0.10, and 0.20), but this may be due to slight inaccuracies in viscosity estimates due to the freezing method used.

Parenthetically, it is interesting to note that at low speeds, extrapolated values of the empirical correlation deviate substantially from the theory of Equation (20); $\overline{T}/_{Go}$ values are 27% and 64% lower than theory at N_{Ca} of 0.01 and 0.001, respectively. Furthermore, Equation (20) indicates that the slope of $(\log \overline{T}/\log N_{Ca})$ and $(\log \overline{h}/R)/(\log N_{Ca})$ was dependent on the region of N_{Ca} selected by Goucher and Ward for their experiments. In hindsight, therefore, it seems quite fortuitous that the region selected happened to be that where the slope of $(\log \overline{h}/R)/(\log N_{Ca})$ was closely approximated by unity, resulting in the simple function shown in Equation (6*a*).

SUMMARY

1. A low-speed theory for the cylinder withdrawal process is presented which is general for all wire radii [Equation (12*a*), Table 1, and Figure 7]. It has been substantiated experimentally at N_{Ca} of 0.0001 to 0.03, for all available N_{Go}, and for oily fluids. For smaller wires of $N_{Go} \leq 0.1$, it is valid up to speeds of $N_{Ca} \leq 0.2$. It does not apply at higher speeds.

2. The theory shows that a wire with $N_{Go} > 3$ can be considered a flat plate, thus substantiating the experimental observation of Van Rossum (*7*).

3. The theory shows that small wires with $N_{Go} < 0.06$ can be described by simple analytical expressions [Equations (18) to (20)], which are applicable over a much wider range of N_{Ca} than Goucher and Ward's empirical correlation (*2*).

ACKNOWLEDGMENT

This work was supported by Grant G-19820 from the National Science Foundation and a fellowship from the Standard Oil Company of California.

NOTATION

a = capillary length, $(2\sigma/\rho g)^{1/2}$
g = gravitational acceleration
h_o = film thickness, $s_o - R$
$\overline{h}$ = flux thickness, $\overline{s} - R$
$L_o, \overline{L}$ = low-speed theory, Equations (13) and (16)
N_{Ca} = capillary number (dimensionless speed), $\mu u_w/\sigma$
N_{Go} = Goucher number (dimensionless radius), R/a
Q = volume of liquid entrained, defined by Equation (1)
r = radial coordinate
R = wire radius
s = film radius at any point

s_o = film radius in the constant-with-height region
$\bar{s}$ = flux radius, defined by Equation (3)
T_o = dimensionless thickness, $(s_o - R)(\rho g/\mu u_w)^{1/2}$
$\bar{T}$ = dimensionless flux, defined by Equation (4) or (15)
u = vertical fluid velocity
u_w = wire withdrawal speed
x = vertical coordinate

Greek Letters

μ = viscosity
π = 3.14159
ρ = density
σ = surface tension at the liquid-gas interface

LITERATURE CITED

1. Derayagin, B. V., and A. S. Titiyevskava, *Dokl. Akad. Nauk. SSSR*, **50**, 307 (1945).
2. Goucher, F. S., and H. Ward, *Phil. Mag.*, 6th Ser., **44**, 1002 (1922).
3. Landau, L. D., and V. G. Levich, *Acta Physiochem. U. R. S. S.*, **17**, No. 1-2, 41 (1942).
4. Levich, V. G., "Physicochemical Hydrodynamics," Chapt. 12, Prentice Hall, New York (1962).
5. Tallmadge, J. A., Ontario Waste Treatment Conf., Ontario Water Res. Comm., Canada, **11**, 121 (1964).
6. ———, R. A. Labine, and B. H. Wood, *Ind. Eng. Chem. Fundamentals Quart.*, **4**, 400 (1965).
7. Van Rossum, J. J., *Appl. Sci. Res.*, **A7**, 121 (1958).
8. White, D. A., Ph.D. dissertation, Yale Univ., New Haven (April, 1965).
9. ———, and J. A. Tallmadge, *J. Fluid Mech.*, **23**, 325 (1965).
10. ————, *Chem. Eng. Sci.*, **20**, 33 (1965).

Manuscript received June 8, 1965; revision received October 25, 1965; paper accepted October 29, 1965.

Binary Physical Adsorption of Argon and Nitrogen on Fixed Beds of Activated Silica Gel

DAVID T. CAMP and LAWRENCE N. CANJAR

Carnegie Institute of Technology, Pittsburgh, Pennsylvania

The physical adsorption and desorption of argon and nitrogen on fixed beds of 18 × 20 mesh silica gel at —78.5°C. and 1 atm. have been studied. Binary mixtures containing 5.52, 10.34, 51.0, 90.16, 95.13 mole % nitrogen, as well as pure argon and pure nitrogen, were used. Superficial gas velocities were varied from 0.10 to 0.27 ft./sec. Concentration vs. time curves were obtained at bed depths of 5.3, 8.6, and 12.0 in.

Resistance to mass transfer from the gas stream to the outside surface of the particles was found to be negligible. The rate is limited due to mass transfer from the outside surface to the internal surface of the particle. The data were correlated by the integrated Rosen diffusion solution with $D = 9.60\ (10^{-8})$ sq.ft./sec. or alternatively, by the Hiester and Vermeulen integrated model with $k_p = 0.23$ sec.$^{-1}$.

Despite the industrial importance of physical adsorption, information necessary for the accurate design of fixed bed adsorbers is scarce. There is considerable uncertainty in the molecular mechanism of this phenomenon. The rate data that have been obtained in the past have been correlated, in general, in an empirical manner and therefore are of limited applicability. Furthermore, little has been done concerning the practical situation where there is appreciable adsorption of more than one component. This research was undertaken to determine the proper form of the rate equation to be expected when both components of a binary mixture are adsorbed to an appreciable extent. With such a rate equation, an equilibrium relationship for the distribution of material between the gas and adsorbed state, and a material balance, one can, either analytically or by numerical techniques compute breakthrough curves. This approach would place the design of such fixed-bed units on a more fundamental basis than the empirical scale-up techniques in current use.

Lawrence N. Canjar is at the University of Detroit, Detroit, Michigan.

EXPERIMENTAL PROCEDURE

Except for several modifications, the equipment was the same as that used by Geser (*1*). A schematic drawing of the apparatus is shown in Figure 1. Cylinders containing argon and prepurified nitrogen, as well as mixtures of these gases, were used. Minimum purities were 99.9% for argon and 99.996% for nitrogen. The available mixtures were analyzed as 4.87, 9.84, 49.0, 89.66, and 94.48% argon. In each run, two cylinders of gas were used, one pure and one a mixture. As shown in Figure 1, gas from either of the cylinders flowed in ¼-in. stainless steel tubing through the gas selector switch, metering valves, a rotameter, and then into a thermostat maintained at —78.5°C. by a bath of methylene chloride and dry ice. The gas was then cooled to the bath temperature by approximately 65 ft. of tubing and entered the adsorption cell.

It flowed first into a 15-in. long auxiliary adsorption tube connected to the base of the main part of the adsorption vessel. The gas then entered the main part which consisted of two 6-in. long adsorption tubes connected by three flanges, one at the effluent end of each adsorption tube. The auxiliary tube was longer than the main tubes to permit establishment of the profile shape. The vessel was sealed by beveled metal-